Int. J. Electrochem. Sci., 15 **(2020)** 1437 – 1449, doi: 10.20964/2020.02.27

International Journal of
ELECTROCHEMICAL
SCIENCE
www.electrochemsci.org

2-(3H-Imidazol-4-yl)-ethylamine as a Green Corrosion Inhibitor for Q235 Steel in Hydrochloric Acid

Jinliang Zhang

School of Materials and Chemical Engineering, Ningbo University Of Technology, Ningbo, Zhejiang 315211, China
E-mail: zhangjinliang_nut@163.com

Received: 8 September 2019 / *Accepted:* 25 October 2019 / *Published:* 31 December 2019

2-(3H-Imidazol-4-yl)-ethylamine (HIE) was researched as a green novel corrosion inhibitor for Q235 steel in 1 M HCl. In this work, electrochemical methods, surface morphology analysis, and theoretical calculations were used to explore the corrosion inhibition performance of HIE. Electrochemical results show that HIE can exhibit superior anti-corrosion performance for Q235 steel in HCl. SEM and AFM intuitively prove that HIE can effectively inhibit the corrosion of Q235 steel. In addition, it is worth mentioning that the adsorption of HIE on the Q235 steel surface is consistent with Langmuir isotherm adsorption. The quantum chemical calculations and molecular dynamics simulations had demonstrated that HIE exhibits excellent corrosion inhibition performance.

Keywords: 2-(3H-Imidazol-4-yl)-ethylamine; Q235 steel; hydrochloric acid; corrosion inhibitor; Langmuir isotherm adsorption; molecular dynamics simulations

1. INTRODUCTION

Q235 steel is a kind of ordinary carbon structural steel. It has excellent properties such as plasticity, toughness, hardness, strength and welding. Therefore, it is widely used in construction machinery, weaponry, resource and environment, energy and power, marine applications and other fields [1-3]. However, in most cases, steel is inevitably affected by environmental factors such as light, temperature, pH, and microorganisms during the application process. Its structure and properties are easily damaged, and many large steel equipment cannot work properly. Therefore, anti-corrosion research on Q235 steel has been receiving much attention.

Among many metal protection methods, corrosion inhibitors are one of the low cost and convenient methods [4-7]. Adding corrosion inhibitor is a good process with wide application, simple process and low cost in metal corrosion protection, especially for power, transportation, metallurgy and other fields [8, 9]. Hydrochloric acid is commonly used in industrial pickling processes [10]. It is often

necessary to add inhibitors to control the consumption of iron and iron alloys and to reduce the amount of acid used. It has been reported that organic corrosion inhibitor molecules containing polar groups such as nitrogen, oxygen, sulfur, unsaturated bonds and aromatic rings can be adsorbed on metal surfaces by electrostatic interaction or coordination covalent bond [11-17].

In recent years, research on environmentally friendly corrosion inhibitors has become a hot spot in corrosion research. Tan et al. [18] studied the anti-corrosion properties of two food flavors on steel in sulfuric acid solution. Experimental and theoretical calculations showed that the two food flavors can exhibit excellent corrosion inhibition performance. Wang et al. [19] studied ficus tikoua leaves extract as an eco-friendly corrosion inhibitor for carbon steel in HCl. It can be clearly found that they are all natural environmentally friendly corrosion inhibitors. In my work, HIE naturally exists in papaya fruit. Therefore, HIE is a green corrosion inhibitor. I used a combination of experimental and theoretical calculations to deeply investigate the anti-corrosion performance of HIE for Q235 steel in 1 M HCl.

2. EXPERIMENTAL

2.1 Material preparation

HIE purchased from Adama Reagent, which has a purity greater than 99.5%. The chemical structure of HIE is shown in Figure 1. It can be found that its molecular formula consists of a nitrogen-containing five-membered ring and an amino group. So it is a relatively stable structure. The chemical composition of Q235 steel is listed in Table 1. The Q235 steel was cut into 1×1×1 cm^3 samples for preparation of working electrodes. The other side of the Q235 steel electrode was sealed with oxidized resin, leaving a 1×1 cm^2 working surface. HIE was formulated into a concentration gradient of 0.5, 1, 2, and 5 mM for electrochemical testing.

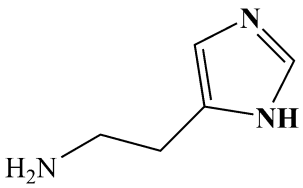

Figure 1. Molecular structure of HIE.

Table 1. Chemical composition of Q235 steel

Elements	Fe	Mn	Si	S	C	P
Proportion	99.44 %	0.14 %	0.17 %	0.04 %	0.17 %	0.04 %

2.2 Electrochemical experiments

The electrochemical experiments of this research were executed at the Chi660e electrochemical workstation (Shanghai Chenhua Co., Ltd.) with a traditional three-electrode system at the temperature

of 298 K. Q235 steel was the working electrode. At each test, carefully polish the Q235 electrode on 180 to 3000 mesh sandpaper. The platinum electrode was an auxiliary electrode. Its area is 2×2 cm^2. Saturated calomel electrode (SCE) was reference electrode. Firstly, the open circuit potential test was performed and the test time was 1800 seconds. The initial potential was the stable open circuit potential value (Eocp), the frequency scope was 100 kHz to 10 mHz, and the sinusoidal excitation signal wave was 10 mV. Finally, the polarization curve was tested. The range of polarization was Eocp ± 0.25 V, and the scanning rate was 0.01 mV/s.

2.3 Surface topography test

The Q235 steel was cut into 1×1×1 cm^3 and 0.5×0.5×0.5 cm^3 samples for AFM (MFP-3D-BIO) and SEM (JEOL-JSM-7800F) testing, respectively. Prior to testing, Q235 steel samples were sequentially sanded on sandpapers of 180 to 7000 mesh. The polished Q235 steel samples were immersed in hydrochloric acid solution with and without 5 mM HIE for 2 hours at 298 K.

2.4 Theoretical calculation

The quantum chemical calculations and molecular dynamics simulation (MDS) of HIE molecules are performed in Material Studio 8.0 software. The calculated parameter settings were as following: The task of calculation was structural optimization. Quality was medium. Energy was 4×10^{-5} Ha. Max.force was 0.05 Ha/Å. Basis Set and Basis file were DNP and 4.4, respectively. Forcefield was the COMPASS force field. The adsorption configuration of HIE and 500 H_2O molecules on the Fe (110) surface was calculated in the forcite module of MS 8.0 software. The parameters were set as following: the calculated task was Dynamics. Qualit was medium. Ensemble was NVT. Time step was 1fs, and Total simulation time was 1000 ps.

3. RESULTS AND DISCUSSION

3.1 Electrochemical impedance spectroscopy (EIS)

Figure 2 is an electrochemical impedance spectroscopy (EIS) of Q235 steel in 1 M hydrochloric acid solution at different HIE concentrations in the 298 K. In Figure 2(a), we can see that the capacitive loop arc shows a depressed semicircle, which can be attributed to the adsorption of HIE molecules on the surface of Q235 steel, resulting in uneven surface of the steel electrode. It is also worth mentioning that with the HIE concentration increases, the radius of the capacitive loop arc increases significantly, indicating an increase in charge transfer resistance. That is to say, the corrosion resistance of Q235 steel is increased due to the adsorption of HIE on the steel surface.

In Figure 2(b), it can be found that the impedance modulus of the low frequency region when the addition of 5 mM HIE is significantly increased by an order of magnitude for the blank solution. Since the low frequency region corresponds to diffusion control, this indicates that the adsorption of HIE

causes the diffusion of iron ions into the solution to be significantly weakened. In addition, the plot of the phase angle value after adding HIE is significantly larger and wider. This shows that HIE can show excellent corrosion inhibition performance.

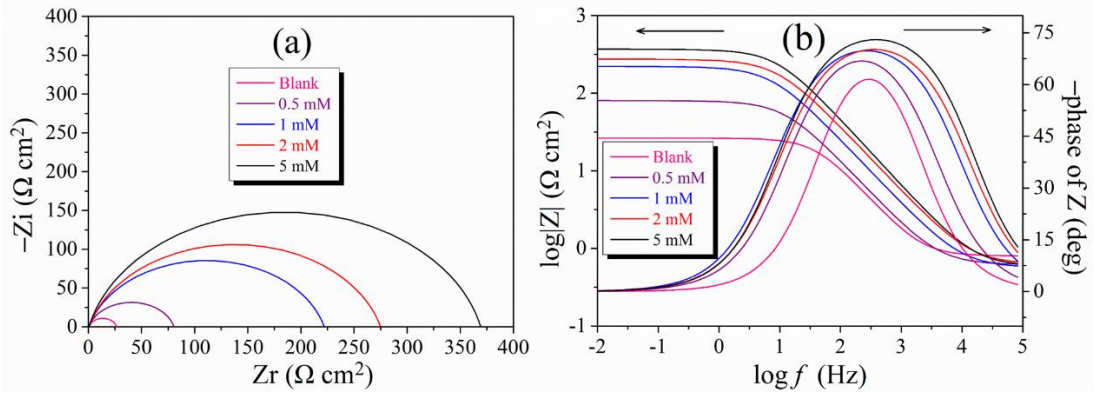

Figure 2. The electrochemical impedance spectroscopy (EIS) of Q235 steel in 1 M hydrochloric acid solution at different HIE concentrations in the 298 K: (a) Nyquist plot. (b) Bode plot.

In order to further understand the EIS experimental data, we used the equivalent circuit diagram of Figure 3 to fit the impedance spectrum. The results of the fitting are listed in Table 2. R_S is the solution resistance. R_{ct} is a Charge transfer resistance. n is the deviation index. C_{dl} is an electric double layer capacitor. η is the corrosion inhibition efficiency. The values of η and C_{dl} can be obtained by the following formulas [20-23]:

$$\eta(\%) = \frac{R_{ct} - R_{ct,0}}{R_{ct}} \times 100 \quad (1)$$

$$C = Y_0(\omega)^{n-1} = Y_0(2\pi f_{Z_{im-Max}})^{n-1} \quad (2)$$

the value of $f_{Zim\text{-}Max}$ is the frequency corresponding to the maximum imaginary part of the impedance, $R_{ct,0}$ and R_{ct} are charge transfer resistance without and with HIE, respectively.

From Table 2, we can see that the inhibition efficiency increases significantly with the increase of HIE concentration. When the concentration of HIE is 5 mM, the inhibition efficiency has reached 93.1%. It is also worth mentioning that as the value of the deviation index n appears to approach 1 as the concentration increases. Explain that the surface of the electrode has a capacitive property, which indicates that HIE forms a dense protective film on the surface of Q235 steel. In addition, it can be found that the value of C_{dl} is obviously declining. According to Helmholtz model [24]:

$$C_{dl} = \frac{\varepsilon^0 \varepsilon}{d} S \quad (3)$$

where ε and ε^0 stand for the local dielectric constant and the air dielectric constant of the electric double layer, respectively, S is the surface area of the Q235 electrode, and d is the thickness of the electric double layer. The more molecules the HIE molecule replaces the surface of Q235, the more obvious the decrease in the value of C_{dl}.

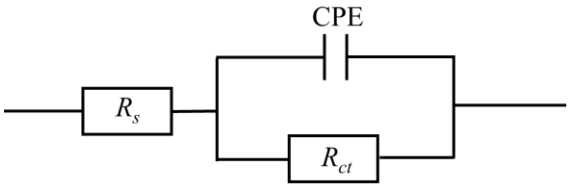

Figure 3. Equivalent circuit diagram for fitting electrochemical impedance spectroscopy.

Table 2. Electrochemical impedance spectroscopy (EIS) of parameters after fitting.

C (mM)	R_s (Ω cm^2)	$Y_0\times10^{-6}$ (S s^n cm^{-2})	n	C_{dl} (μF cm^{-2})	R_{ct} (Ω cm^2)	η (%)
Blank	0.57	170.5	0.90	120.37	25.6	-
HIE						
0.5	0.53	85.9	0.93	60.9	79.8	67.9
1	0.62	55.3	0.96	56.1	221.4	88.4
2	0.51	52.0	0.98	46.0	274.3	90.6
5	0.70	48.3	0.99	35.1	368.6	93.1

3.2 Potentiodynamic polarization (PDP) curves

Figure 4 shows the polarization curve of Q235 steel in 1 M hydrochloric acid solution at 298 K with various HIE concentrations. It can be found that as the concentration of HIE increases, the corrosion current density shows a declining trend. This indicates that HIE can effectively inhibit the corrosion of Q235 steel in hydrochloric acid solution. The polarization curves of the cathodic branches show a parallel trend, which indicates that the adsorption of HIE molecules in Q235 steel does not change the reaction mechanism of the cathode. While, the slope of the polarization curve of the anode branch changes significantly, which indicates that HIE can effectively inhibit the dissolution of iron ions. It is worth mentioning that at the HIE concentration of 5 mM, the slope of the anode branch increases sharply, indicating that the HIE molecule desorbs on the Q235 steel surface.

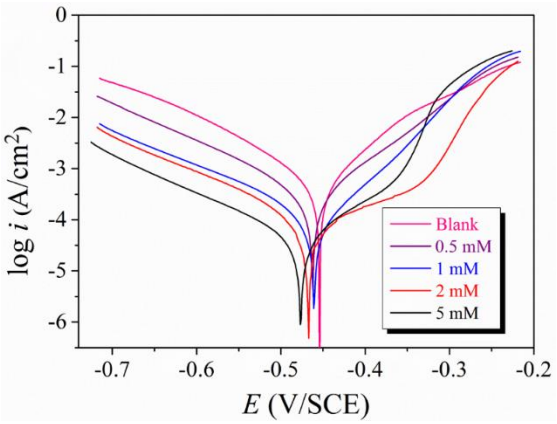

Figure 4. The polarization curve of Q235 steel in 1 M HCl at 298 K with different HIE concentrations.

We used the Tafel extrapolation method to obtain parameters such as corrosion current density and corrosion potential. These parameters are listed in Table 3.

The corrosion current density can be calculated by the following formula [25-33]:

$$\eta(\%) = \frac{i_{corr,0} - i_{coor}}{i_{corr,0}} \times 100 \quad (4)$$

where i_{corr} and $i_{corr,0}$ are corrosion current density with and without HIE, respectively.

After the addition of HIE, the corrosion potential shifts significantly toward the cathode, but the change in corrosion potential is significantly less than 85 mV relative to the blank solution, indicating that HIE is a mixed-type corrosion inhibitor. Besides, it can be found that when the HIE concentration is 5 mM, the corrosion current density drops to 19.4 μA cm^{-2}, and the inhibition efficiency is 96.4%. Therefore, it can be strongly proved that HIE has excellent anti-corrosion performance on Q235 steel in 1 M HCl.

Table 3. Polarization curves parameters

C (mM)	E_{corr}(V/SCE)	i_{corr}(μA cm^{-2})	β_c(mV dec^{-1})	β_a(mV dec^{-1})	η (%)
Blank	–0.454	540.2	–107	83	—
HIE					
0.5	–0.462	158.8	–98	95	70.6
1	–0.461	51.3	–106	107	90.5
2	–0.467	42.6	–110	97	92.1
5	–0.477	19.4	–125	95	96.4

3.3 Scanning electron microscopy

Figure 5 is the surface topography of Q235 steel under different conditions. Figure 5 (a) is the surface topography after grinding. It can be found that the entire Q235 steel surface is very flat, with only a small amount of scratches left after polishing. Figure 5(b) is the surface topography diagram after immersing Q235 in 1 M hydrochloric acid containing 5 mM HIE for 2 hours at 298 K. It can be found that there are a small amount of corrosion holes on the surface, and the scratches left by the polishing are faintly visible. Figure 5 (c) is the surface topography diagram of immersing Q235 steel in 1 M hydrochloric acid without HIE for 2 hours at 298 K. It can be found that the surface of the entire Q235 steel has been severely corroded. By comparing Figures 5(b) and (c), it can be found that HIE can exhibit excellent anti-corrosion performance.

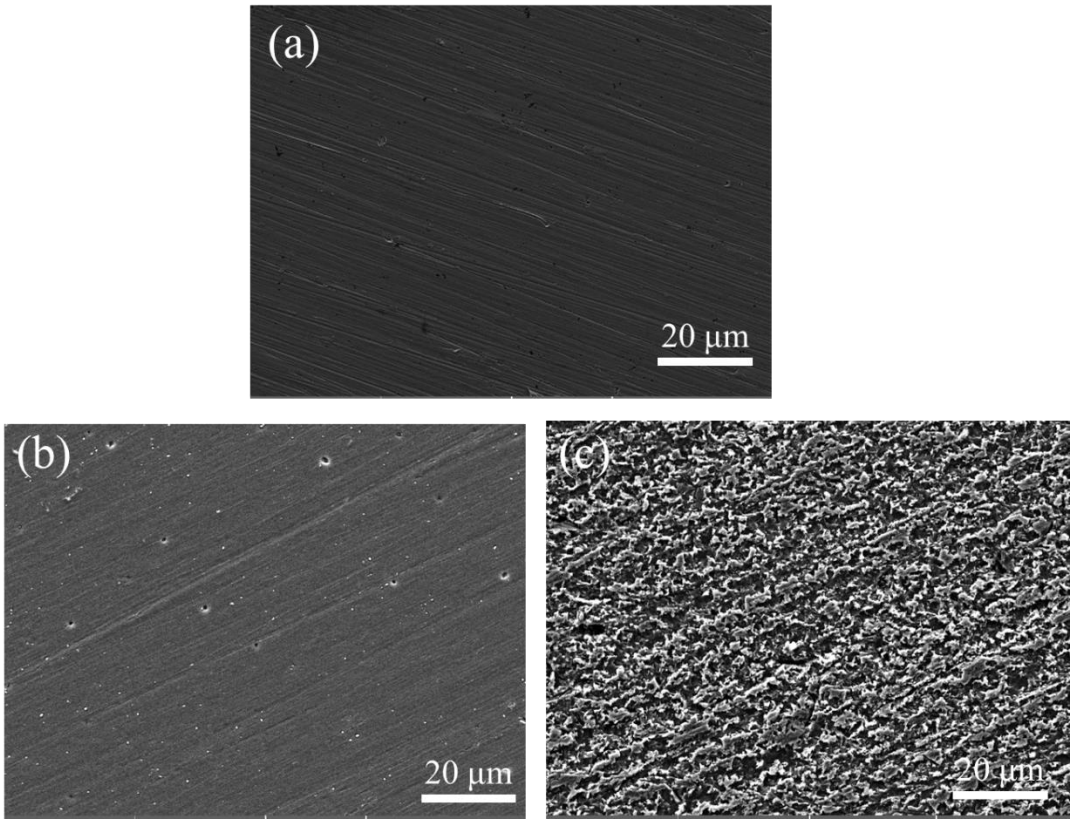

Figure 5. The surface topography of Q235 steel under different conditions: (a) the surface topography after grinding. (b) the surface topography diagram after immersing Q235 in 1 M HCl containing 5 mM HIE for 2 hours at 298 K. (c) the surface topography diagram of immersing Q235 steel in 1 M HCl without HIE for 2 hours at 298 K.

3.4 Atomic Force Microscope

Figure 6 shows an atomic force microscope 3D image under different conditions. Figure 7 is a 2D contour map under different conditions. Figure 6 (a) is the 3D surface topography after grinding. It can be seen that a lot of scratches appear on the entire 5×5 μm^2 surface. After grinding, the surface roughness of Q235 is about 9 nm. Figure 6(b) is the 3D surface topography diagram after immersing Q235 in 1 M hydrochloric acid containing 5 mM HIE for 2 hours at 298 K. In the presence of 5 mM HIE, the surface roughness of Q235 is about 12 nm. Figure 5 (c) is the 3D surface topography diagram of immersing Q235 steel in 1 M hydrochloric acid without HIE for 2 hours at 298 K. The surface roughness of Q235 is about 38 nm. By comparing their roughness, it can be found that HIE can effectively inhibit the corrosion of Q235 in hydrochloric acid solution.

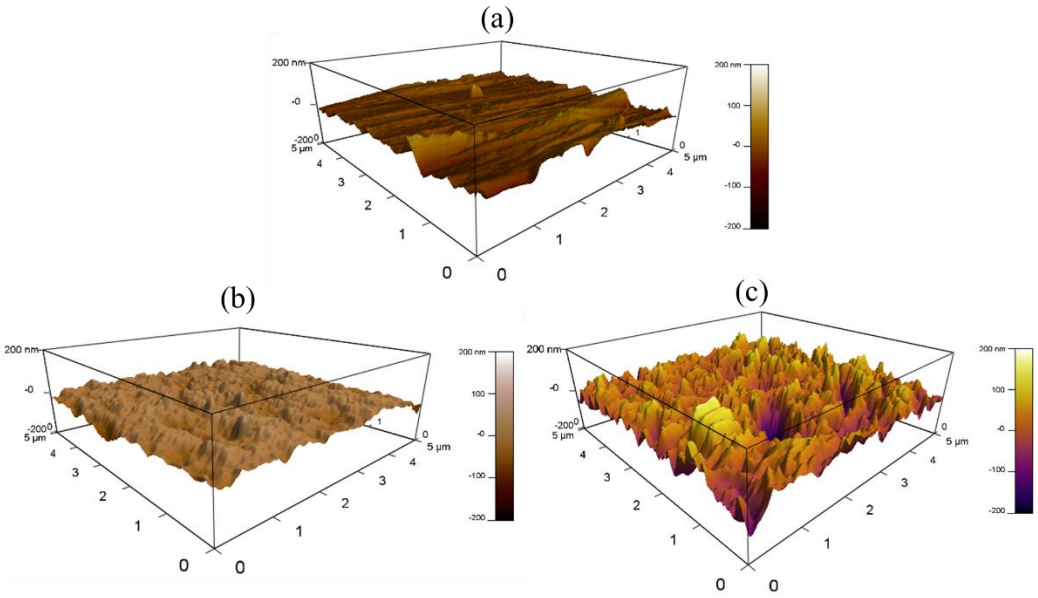

Figure 6. The atomic force microscope 3D image under different conditions. (a) the surface topography after grinding. (b) the surface topography diagram after immersing Q235 in 1 M hydrochloric acid containing 5 mM HIE for 2 hours at 298 K. (c) the surface topography diagram of immersing Q235 steel in 1 M hydrochloric acid without HIE for 2 hours at 298 K.

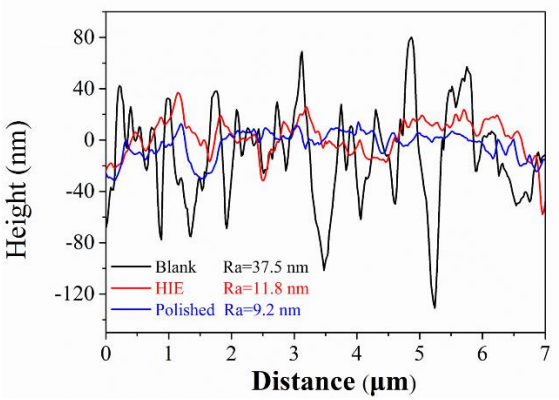

Figure 7. The 2D contour map under different conditions.

3.5 Adsorption isotherm research

In order to study the adsorption of HIE molecules on the surface of Q235 steel. We used different isothermal adsorption models to fit the polarization curve data. The experimental results show that the adsorption of HIE on the surface of Q235 steel is consistent with Langmuir's single layer adsorption. The results of the fit are listed in Figure 8. The fitted linear regression coefficient R^2 is close to 1. It indicates that the adsorption behavior of HIE on the surface of Q235 steel is consistent with Langmuir adsorption. Langmuir adsorption isotherm expression is as following [34]:

$$\frac{\theta}{1-\theta} = K_{ads}C \qquad (5)$$

Where C is the concentration of HIE. K_{ads} is the adsorption equilibrium constant. θ is the coverage. By calculation, it can be concluded that the value K_{ads} is 6348.4 (L/mol).

To further understand the type of adsorption of HIE in Q235 steel. The value of ΔG_{ads}^{0} was calculated using the following formula [35]:

$$K_{ads} = \frac{1}{55.5}\exp(-\frac{\Delta G_{ads}^{0}}{RT}) \qquad (6)$$

where 55.5 is the H_2O molar concentration, R stands for the gas constant, and T is the thermodynamic temperature. The ΔG_{ads}^{0} value of the HIE adsorb on Q235 steel surface is –31.6 kJ/mol. It is well known that the absolute value of ΔG_{ads}^{0} is less than 20 kJ/mol, indicating that there is only physical adsorption. The absolute value of ΔG_{ads}^{0} greater than 40 kJ/mol indicates the presence of only chemisorption. When the value of ΔG_{ads}^{0} is between 20 and 40 kJ/mol, there is a physical and chemical adsorption coexisting [35, 36]. Therefore, it can be proved that the adsorption of HIE on the surface of Q235 steel has a combination of physical and chemical adsorption.

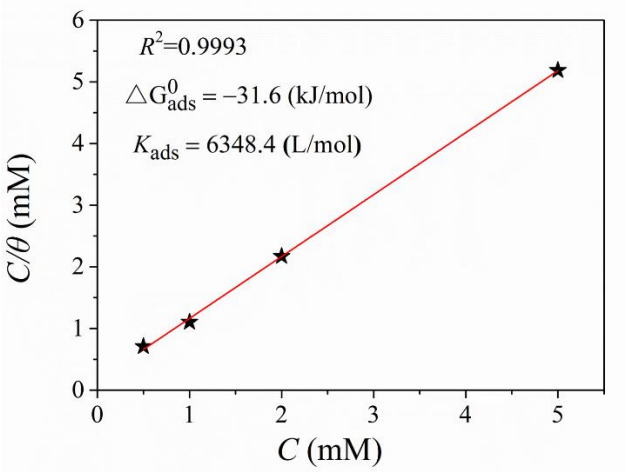

Figure 8. Fitted results of Langmuir isothermal adsorption.

3.6 Quantum chemistry calculation

Quantum chemical calculation is an effective way to predict the corrosion inhibition of corrosion inhibitor molecules. In this work, we calculated the frontier molecular orbitals, dipole moments, and electrostatic potential maps of HIE molecule. The result of the calculation is presented in Figure 9.

In Figure 9, it can be found that the electrostatic potential map of HIE consists of a red region and a blue region. The red region is mainly distributed on the five-membered ring containing nitrogen atoms and the nitrogen atom. While, the blue area is mainly distributed on carbon atoms. The red color of the ESP map has a nucleophilic nature, and the blue regions are electrophilic nature [18]. Therefore, it can be proved that HIE participates in chemical bonding with Q23 steel mainly through nitrogen-containing heteroatoms and nitrogen-containing five-membered rings.

Frontier molecular orbital theory is widely used to study the electron cloud density distribution of corrosion inhibitor molecules. It can effectively determine the active site of the inhibitor molecule. In Figure 9, it can be found that the electron cloud density of the HIE molecule is uniformly distributed over the entire molecule. This indicates that HIE molecules are more likely to adsorb in parallel on the surface of Q235 steel.

In addition, we calculate the values of dipole moment and energy gap ($\Delta E = E_{LUMO} - E_{HOMO}$) of the HIE molecule [37, 38]. The energy gap value of HIE is 3.17 eV. The dipole moment of HIE is 3.3 Debye. Most corrosion workers believe that small energy gap values and large dipole moments correspond to superior corrosion inhibition performance [39]. We can see that HIE has a small gap value and a large dipole moment. Therefore, it can be judged that HIE molecules can show excellent corrosion inhibition performance. This is consistent with the experimental results.

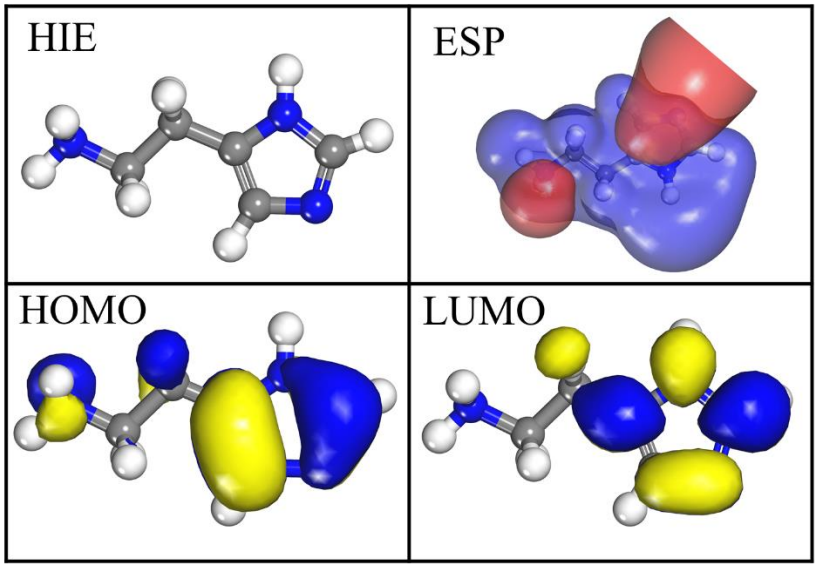

Figure 9. Results of quantum chemical calculations including HIE-optimized configuration, electrostatic potential map, and electron cloud distribution of frontier molecular orbitals, respectively.

3.7 Molecular dynamics simulation

Molecular dynamics simulation (MDS) can effectively calculate the adsorption behavior of corrosion inhibitor molecules on metal surface. Figure 10 presents the stable adsorption configuration of HIE molecules on the surface of Fe(110) surface. It can be found that the HIE molecules are adsorbed almost parallel on the Fe(110) surface through the nitrogen-containing five-membered ring and the nitrogen hetero atom. This is consistent with the results of previous quantum chemical predictions. In addition, we obtained the binding energy of HIE molecules on the surface of Q235 steel by the following formulas [39]:

$$E_{binding} = -E_{\text{int}\,eract} \quad (7)$$

$$E_{\text{int}\,eract} = E_{tot} - (E_{subs} + E_{inh}) \quad (8)$$

where $E_{binding}$ represents the binding energy of HIE and Q235 steel surface, E_{tot} represents the total energy of the entire simulation system, E_{subs} represents the total energy of the Fe(110) and H_2O, and E_{inh} represents the energy of the HIE molecule. The binding energies of HIE on the surface of Q235 steel is 337.9 kJ/mol. This indicates that the HIE molecule has a strong adsorption capacity on the surface of Q235 steel, thus exhibiting excellent corrosion inhibition performance.

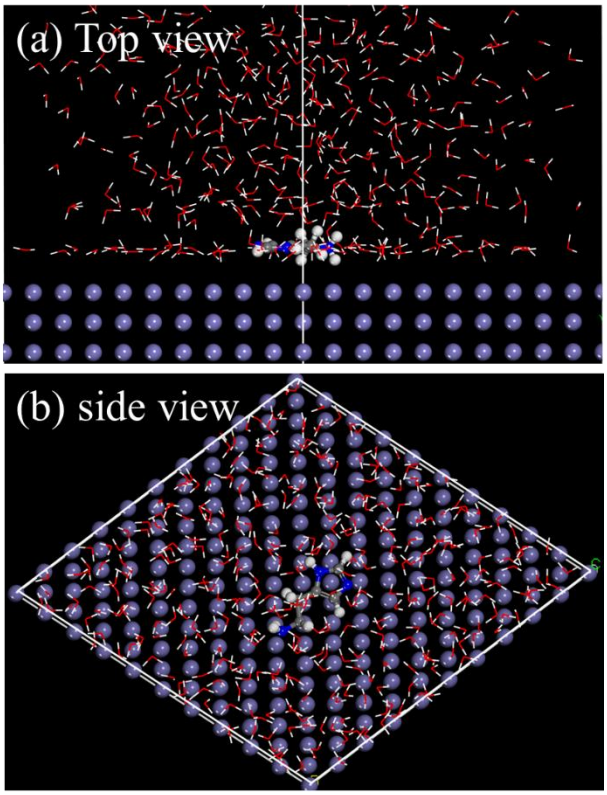

Figure 10. Stable configuration of HIE adsorbed on the Fe(110) plane; (a) top view, (b) side view.

4. CONCLUSION

HIE molecule exhibits excellent corrosion inhibition performance of Q235 steel in 1 M HCl. Electrochemical experiments show that HIE molecules can simultaneously inhibit the cathodic and anodic reaction of Q235, which is a mixed-type corrosion inhibitor. Significant desorption behavior at the anode branch when the HIE concentration is 5 mM. SEM and AFM morphology analysis strongly and vividly corroborate the results of electrochemical tests. The adsorption of HIE on Q235 steel surface is consistent with Langmuir's single layer adsorption. Its adsorption type is a combination of physicochemical adsorption. Quantum chemical calculations strongly explore the active adsorption sites of HIE molecule. Molecular dynamics simulations show that HIE molecules can be adsorbed in parallel on the Fe(110) surface to obtain the largest coverage area.

References

1. X. Zhang and B. Tan, *Int. J. Electrochem. Sci.,* 13 (2018) 11388.
2. Y.J. Yang, Y. Li, L. Wang and H. Liu, D.M. Lu, L. Peng, *Int. J. Electrochem. Sci.,* (2019) 3375.
3. M.R. Zahra Sanaei, Ghasem Bahlakeh and Bahram Ramezanzadeh, *J. Ind. Eng. Chem.,* 69 (2019) 18.
4. B. Tan, S. Zhang, W. Li, X. Zuo, Y. Qiang, L. Xu, J. Hao and S. Chen, *J. Ind. Eng. Chem.,* 77 (2019) 449.
5. S. Tao and H. Huang, *Int. J. Electrochem. Sci.,* 14 (2019) 5435.
6. T. Douadi, H. Hamani, D. Daoud, M. Al-Noaimi and S. Chafaa, *J. Taiwan Inst. Chem. E.,* 71 (2017) 388.
7. C. Wang, W. Gou, C. Liu, D. Fu, L. Zhou, C. Lai, B. Xie and S. Zhu, *Int. J. Electrochem. Sci.,* (2019) 3443.
8. F. El-Hajjaji, M. Messali, M.V. Martinez de Yuso, E. Rodriguez-Castellon, S. Almutairi, T.J. Bandosz and M. Algarra, *J. Colloid Interf. Sci.,* 541 (2019) 418.
9. P.E. Alvarez, M.V. Fiori-Bimbi, A. Neske, S.A. Brandán and C.A. Gervasi, *J. Ind. Eng. Chem.,* 58 (2018) 92.
10. Y. Yang, H. Liu, D.M. Lu, L. Peng and L. Wang, *Int. J. Electrochem. Sci.,* 14 (2019) 3375.
11. M. M. Antonijevic and M. B. Petrovic, *Int. J. Electrochem. Sci.,* 3 (2008) 1.
12. B. Tan, S. Zhang, Y. Qiang, L. Guo, L. Feng, C. Liao, Y. Xu and S. Chen, *J. Colloid Interf. Sci.,* 526 (2018) 268.
13. Samar .Y. Al-Nami, *Int. J. Electrochem. Sci.,* 14 (2019) 3986.
14. S. Xu, W. Li, X. Zuo, D. Zheng, X. Zheng and S. Zhang, *Int. J. Electrochem. Sci.,* 14 (2019) 5777.
15. A. Singh, K.R. Ansari, J. Haque, P. Dohare, H. Lgaz, R. Salghi and M.A. Quraishi, *J. Taiwan Inst. Chem. E.,* 82 (2018) 233.
16. S. Javadian, B. Darbasizadeh, A. Yousefi, F. Ektefa, N. Dalir and J. Kakemam, *J. Taiwan Inst. Chem. E.,* 71 (2017) 344.
17. P. Kannan, T.S. Rao and N. Rajendran, *J. Colloid Interf. Sci.,* 512 (2018) 618.
18. B. Tan, S. Zhang, H. Liu, Y. Guo, Y. Qiang, W. Li, L. Guo, C. Xu and S. Chen, *J. Colloid Interf. Sci.,* 538 (2019) 519.
19. Q. Wang, B. Tan, H. Bao, Y. Xie, Y. Mou, P. Li, D. Chen, Y. Shi, X. Li and W. Yang, *Bioelectrochemistry,* 128 (2019) 49.
20. B. Tan, S. Zhang, Y. Qiang, L. Feng, C. Liao, Y. Xu and S. Chen, *J. Mol. Liq.,* 248 (2017) 902.
21. N. Chafai, S. Chafaa, K. Benbouguerra, D. Daoud, A. Hellal and M. Mehri, *J. Taiwan Inst. Chem. E.,* 70 (2017) 331.
22. M. Ramezanzadeh, Z. Sanaei, G. Bahlakeh and B. Ramezanzadeh, *J. Mol. Liq.,* 256 (2018) 67.
23. X. Wang, H. Jiang, D. Zhang, L. Hou and W. Zhou, *Int. J. Electrochem. Sci.,* 14 (2019) 1178.
24. F. El-Hajjaji, M. Messali, A. Aljuhani, M.R. Aouad, B. Hammouti, M.E. Belghiti, D.S. Chauhan and M.A. Quraishi, *J. Mol. Liq.,* 249 (2018) 997.
25. B. Tan, S. Zhang, H. Liu, Y. Qiang, W. Li, L. Guo and S. Chen, *J. Taiwan Inst. Chem. E.,* 102 (2019) 424.
26. M.B. Radovanović and M.M. Antonijević, *J. Adhes. Sci. Technol.*, 31 (2016) 369.
27. Z.Z. Tasic, M.M. Antonijevic, M.B. Petrovic Mihajlovic and M.B. Radovanovic, *J. Mol. Liq.,* 219 (2016) 463.
28. A. S. Fouda, M.M. Hegazi and A. El-Azaly, *Int. J. Electrochem. Sci.,* 14 (2019) 4668.
29. N.D. Nam, P.V. Hien, N.T. Hoai and V.T.H. Thu, *J. Taiwan Inst. Chem. E.,* 91 (2018) 556.
30. M.M. Solomon, S.A. Umoren, M.A. Quraishi and M. Salman, *J. Colloid Interf. Sci.,* 551 (2019) 47.
31. K. Zhang, W. Yang, B. Xu, Y. Chen, X. Yin, Y. Liu and H. Zuo, *J. Colloid Interf. Sci.,* 517 (2018) 52.

32. B.R. M. Motamedi and M. Mahdavian, *J. Ind. Eng. Chem.,* 66 (2018) 116.
33. P.R. Charitha B P, *J. Ind. Eng. Chem.,* 58 (2018) 357.
34. A. Mishra, C. Verma, H. Lgaz, V. Srivastava, M.A. Quraishi and E.E. Ebenso, *J. Mol. Liq.,* 251 (2018) 317.
35. A. Biswas, P. Mourya, D. Mondal, S. Pal and G. Udayabhanu, *J. Mol. Liq.,* 251 (2018) 470.
36. B. Tan, S. Zhang, Y. Qiang, W. Li, H. Liu, C. Xu and S. Chen, *J. Mol. Liq.,* 286 (2019) 110891.
37. Z. Xiao, Z. Zhou, L. Song, D. Wu, C. Zeng and Z. Cao, *Int. J. Electrochem. Sci.*,14 (2019) 4705.
38. J. Tang, Y. Hu, H. Wang, Y. Zhu, Y. Wang, Z. Nie, Y. Wang and B. Normand, *Int. J. Electrochem. Sci.,* 14 (2019) 2246.
39. J. Zhang, L. Zhang and G. Tao, *J. Mol. Liq.,* 272 (2018) 369